Materials Chemistry and Physics 219 (2018) 376–389

Contents lists available at ScienceDirect

Materials Chemistry and Physics

journal homepage: www.elsevier.com/locate/matchemphys

Facile synthesis of rod-shaped bismuth sulfide@graphene oxide (Bi_2S_3@GO) composite

N.-G. García-Peña[a], D. Díaz[a,*], G. Rodríguez-Gattorno[b], I. Betancourt[c], I. Zumeta-Dubé[a,1]

[a] Facultad de Química, Universidad Nacional Autónoma de México, Ciudad de México, 04510, Mexico
[b] Centro de Investigación y de Estudios Avanzados del Instituto Politécnico Nacional-Unidad Mérida, Antigua carretera a Progreso Km. 6, Cordemex Loma Bonita Xcumpich, 97310, Mérida, Yucatán, Mexico
[c] Instituto de Investigaciones en Materiales, Universidad Nacional Autónoma de México, Ciudad de México, 04510, Mexico

HIGHLIGHTS

- The synthesis of a Bi_2S_3@GO composite is proposed using a faster and easier method.
- Bi_2S_3 on GO grows as rods, which tends to grow along the [0 1 0] axis.
- Oxygen functional groups in GO appear to bias the formation of rod-shaped Bi_2S_3.
- Layers of GO wrapping Bi_2S_3 rods were undoubtedly identified by HR-TEM analyses.
- Spherical NPs were achieved when pure Bi_2S_3 was obtained under the same conditions.

GRAPHICAL ABSTRACT

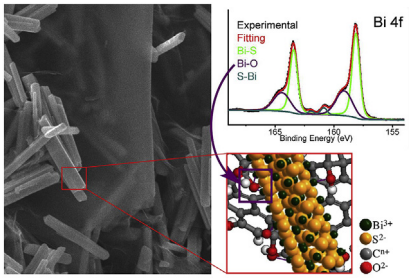

ARTICLE INFO

Keywords:
Graphene oxide
Bismuth sulfide
Bismuth sulfide-graphene oxide composites
Rod-shaped particles
Graphene oxide TEM assays

ABSTRACT

The preparation of rod-like bismuth sulfide structures, effectively anchored to graphene oxide (GO) sheets, is informed using a fast and trouble-free method. This strategy, which incorporates elemental sulfur as S^{2-} source, hot dimethylsulfoxide as solvent, and a short reaction time, has been used to obtain Bi_2S_3@GO composites. The products were characterized by powder-XRD, Raman Spectroscopy, electron absorption spectroscopy in UV–vis–NIR region, SEM, HR-TEM, and XPS. All the characterization techniques showed pure, well-structured, rod-shaped Bi_2S_3 particles with sizes around 150 nm in diameter and hundreds of nanometers in length, which were anchored parallel to graphene oxide matrix. These elongated structures tended to grow along the [0 1 0] axis. Noteworthy, the presence of GO was undoubtedly detected on the surface of elongated bismuth sulfide by HR-TEM assays. In order to test the GO effect on the formation of the rod-like structures, a sample of pristine Bi_2S_3 was synthesized under the same conditions. XPS results indicate the presence of oxygen functional groups in GO as the main factor for the development of the lengthen bismuth sulfide structures, achieving this through the formation of Bi−O bonds.

* Corresponding author. Postal address. Circuito Exterior S/N, Coyoacán, Cd. Universitaria, CP: 04510, Ciudad de México, Mexico.
E-mail addresses: gapenig@gmail.com (N.-G. García-Peña), david@unam.mx (D. Díaz).
[1] Present Address: Unidad Profesional Interdisciplinaria en Ingeniería y Tecnologías Avanzadas, Av. Instituto Politécnico Nacional 2580, La Laguna Ticomán, 07340 Ciudad de México, Ciudad de México, México.

https://doi.org/10.1016/j.matchemphys.2018.08.052
Received 27 March 2018; Received in revised form 16 August 2018; Accepted 18 August 2018
Available online 22 August 2018

1. Introduction

Bismuth sulfide (Bi_2S_3) is a *p*-type semiconductor [1] with a narrow direct band gap or 1.3 eV [1–3] whose structure consists of a lamellar arrangement of alternate Bi^{3+} and S^{2-} infinite chains [2] that tends to crystalize in an orthorhombic system [1–3].

The utility of this compound lies on its properties like charge carrier mobility, structural flexibility or light absorption capacity [4], which make it a promising specie for a number of applications. However, there are a considerable number of studies devoted to photocatalytic applications of Bi_2S_3, many of them devoted to degradation of pigments [5], such as methylene blue [6,7], malachite green [4], acid black [8].

The majority of the methods used to obtain Bi_2S_3 are based on either autoclave-solvothermal [1,5,9–12] or autoclave-solvothermal polyol [13] techniques. Some other techniques such as: microwave-assisted [14], sonochemical-assisted [15], and liquid phase method [16–18] were also found. However, all these methods require long reaction times, high temperatures, pressures and/or great energy consumption. For this reason, it was chosen an early developed technique by Zumeta et al., which employs only 30 min of reactions and temperatures below 120 °C, under room pressure [19,20].

Regarding the sulfide sources, we found that Na_2S salt [2,10,18] and $Na_2S_2O_3$ salt [15] are the most popular. However, these sodium salts have the disadvantage that during the firsts hours of reaction they produce a binary sodium-bismuth sulfide ($NaBiS_2$) product [19,20]. And in order to convert this mixed sulfide species into pure Bi_2S_3 it is necessary to apply extensive reaction times (72 h), temperatures of 160 °C, and pressure higher than the atmospheric (using autoclave) [20]. Other less used sulfide sources, which do not present the aforementioned problem, are CS_2 [13,21,22], thioacetamide [23], and thiourea [5,14]. However, these compounds are either toxic/carcinogenic and difficult to manipulate. Thus, in the present investigation it was chosen elemental sulfur as a sulfide source; since is cheaper, easier to handle, and it allows softer reaction conditions [19,20], despite the fact that only very few researches employ this reactant [3,20], and it is mostly involved in solid-state reactions [3,24].

There are comparatively few examples of synthesis of Bi_2S_3 on reduced graphene oxide (rGO) [9,11,12,25,26] or nitrogen modified-graphene oxide (NG) [27] composites. Nevertheless, we located just one publication where graphene oxide was used without GO reduction step, as support for bismuth sulfide particles [28]. In this case, the synthesis method chosen included an autoclave-hydrothermal technique and poly (3,4-ethylenedioxythiophene) polymer as scaffold agent. Hence, we selected an easier method, which does not require extensive reaction times or harsh conditions.

In literature, there are noteworthy methods to obtain 1D rod-like, ribbons, or wire structures with the aforementioned techniques [1,3,12,13]. It has been argued that the anisotropic habit of Bi_2S_3 nanorods is due to the existence of infinite chains of Bi and S ions one on top of other directed along the [0 0 1] axis in *Pcnm* space group [3], in an orthorhombic Bi_2S_3 cell structure. Some authors emphasize the importance on the formation of these S and Bi element pillars, which may be the principal reason for the formation of the detected rods [3], since this parallel growing of atoms would favor elongated structures. Thus, according to recent studies, the only difference between spherical structures and elongated ones would be the concentration of the precursors [1]. In contrast, other researchers propose that the main reason behind the formation of 1D structures would be the utilization of appropriate sulfide precursors which may work as slow, steady, and high release sources of S^{2-} [29,33]. Finally, some other reports argue that the main factor is the employment of suitable supports that are able to stabilize the surface of particles during growing step [13], such as surfactants [1,2,16,30,31] or polymers [9,32], which may act as template agents.

In addition, some researchers claim that the solvent plays an important role on the formation of specific structures [33,34]. During our investigation, it was evident that solvents with −OH groups, as ethanol [5,18,21,33,34] ethylene glycol [13,16,17,27,32] or water [2,6,10,12,15,16,25,28,31], tend to enhance the formation of rod, wire or tubular Bi_2S_3 structures. Capping agents with −OH and carbonyl −OH functional groups also heighten the formation of these assemblies [1,2,16,29,31]. Surprisingly, dimethylformamide (DMF) [4,29,30] and formaldehyde [14], which do not have −OH groups in their skeleton, improve the formation of these elongated structures. However, this behavior might be due to the characteristic hygroscopy of these solvents. In contrast, this comportment was not observed in dimethyl sulfoxide where only spherical particles were reported [20]. Despite all these changes in forms depending on solvents and capping agents, as far as we know, any investigation has shed some light into the previously mentioned preferential growth, and none of them examine the role of graphene oxide during the formation of Bi_2S_3 elongated structures.

The present paper reports an easy method of synthesis to obtain rod-like Bi_2S_3 structures anchored to graphene oxide sheets, suspended in heated DMSO, during 30 min. The samples have been characterized by powder-XRD, Raman, and electronic absorption (in UV–vis–NIR regions) spectroscopies; along with SEM, HR-TEM, and XPS analyses. All the characterization techniques showed pure, well-structured, rod-shaped Bi_2S_3 particles with sizes around 150 nm in diameter and hundreds of nanometers in length, which were anchored parallel to graphene oxide matrix. It was possible to propose a reason behind the formation of these assemblies, which was related to the importance of graphene oxide presence and its functional groups during the formation of bismuth sulfide rod-like structures. Since XPS, HR-TEM, and XRD assays obtained during our investigation strongly suggest that presence of graphene oxide support is the decisive factor in the formation of the rod-like assemblies, through the formation of Bi−O bonds between the GO and the bismuth sulfide structures. These results contrast with most of the studies about the preparation of elongated Bi_2S_3 arrangements.

2. Experimental

2.1. Materials

All the precursors and solvents were reagent grade and were used as received without further purification. Pyrolytic graphite was purchased from B&A Chemicals (98%); sodium nitrate ($NaNO_3$) from Mallinckrodt (99.9%); bismuth nitrate pentahydrate ($Bi(NO_3)_3{\cdot}5H_2O$) from STREM Chemicals (98%); dimethylsulfoxide (DMSO) from Tecsiquim (99.9%); ammonium hydroxide (NH_4OH) concentrated solution (28.3% NH_3), concentrated sulfuric acid (H_2SO_4, 97.3%) and concentrated hydrochloric acid (HCl, 36.5–38% v/v) from J.T. Baker; potassium permanganate ($KMnO_4$) from Merck (99%); hydrogen peroxide solution (H_2O_2, 30% v/v) from Consorcio Químico Mexicano; and elemental sulfur (S_8) from Sigma-Aldrich (99.5%). Deionized water and acetone were used as washing solvents.

2.2. Characterization analysis

X-ray diffraction (XRD) studies of the Bi_2S_3 structures were measured in a Bruker D2-Phaser diffractometer using Cu Kα radiation (10 mA, 30 kV, λ = 1.5418 Å); electronic absorption spectra, in diffuse reflectance mode, were obtained in a Cary-5E Varian; HR-TEM images were acquired at the Centro de Nanociencias y Micro y Nanotecnologías at Instituto Politécnico Nacional, using an aberration corrected cold-field emission Jeol JEM-ARM200CF HRTEM, operated at 200 kV accelerating voltage, and the Fourier analysis have been obtained via the use of freely available JEMS software, version 4.6531 for MacOSX, and DigitalMicrograph software version 2.1 attached at the microscope; whereas scanning electron microscopy (SEM) studies were carried out in a JEOL-SEM 7600F operated at 20 kV; dispersive Raman spectra were acquired in a EZRaman-L-905 (Enwave Optronics) Raman analyzers coupled to a Leica DM300 microscope (with a Leica objective with a

magnification/numerical aperture ratio of 40x/65) using an excitation laser source of 532 nm (maximum power ~400 mW), respectively; finally, X-ray photoemission spectroscopy (XPS) analysis were measured in a ESCA/SAM Perkin-Elmer model 560, with a spot diameter of 400 μm.

2.3. Synthesis of graphene oxide (GO)

Graphene oxide was synthesized following the widely spread Hummers' method [35] with some modifications: 2 g (166.53 mmol) of pyrolytic graphite and 1 g (11.76 mmol) of sodium nitrate ($NaNO_3$) were mixed in concentrated sulfuric acid (H_2SO_4, 100 mL, 1.88 mol). The reaction flask was left in a sodium chloride-water-ice bath during 5 h, until the mixture was stabilized at 2-5 °C. Next, 6 g (37.96 mmol) of potassium permanganate ($KMnO_4$) were added very slowly in order to avoid a significant rise in the reaction temperature. Once the addition finished, the reaction mixture was heated to 42-44 °C and it was maintained at those conditions during 18 h. After that time, 120 mL of water (H_2O) were added to the reaction flask very slowly and kept at constant agitation until the mixture reached room temperature. Following, 30 mL of hydrogen peroxide (H_2O_2, 30% v/v) were added very slowly. The addition caused an increase in the temperature of the mixture along an evolution of gases. The reaction was allowed to settle during 24 h; subsequently, it was centrifuged until a dark brown solid was obtained. The solid was washed with 2 × 30 mL of a concentrated solution of chloride acid (HCl, 36.5–38%). Then, it was extensively washed with water until the pH reached 6. Finally, the product was rinsed with 3 × 50 mL of acetone and left it to dry in vacuum. A grayish-brown solid was obtained.

2.4. Synthesis of rod-shaped Bi_2S_3-GO composites (Bi_2S_3@GO)

Bi_2S_3-GO composite was synthesized according a previously developed method by Zumeta-Dubé et al. [20] with few modifications. 50 mg of graphene oxide (GO) were ultrasonicated in dimethylsulfoxide (DMSO) during 3.5 h. Once the black solid was dispersed in the liquid media, the volume was adjusted to 50 mL to obtain a GO dispersion with a 0.5 mg/mL concentration. To this dispersion, it was added 121.27 mg (0.25 mmol) of bismuth nitrate pentahydrate ($Bi(NO_3)_3{\cdot}5H_2O$) in order to obtain an initial concentration of 5×10^{-3} M of Bi^{3+}. This mixture was tagged as **M1** and was kept under magnetic agitation during 72 h. Subsequently, 20 mL of dimethylsufoxide (DMSO) was heated to 110 ± 2 °C and, once that temperature was reached, 64.12 mg (0.25 mmol) of elemental sulfur was added. After the yellow solid was completely dissolved, **M1** solution was slowly poured into the later hot solution. At this stage a dark mixture has developed. The new mixture was allowed to reach 110 ± 2 °C; then, 5 mL of a concentrated solution of ammonium hydroxide (28.3% NH_3) were added and kept under heating and vigorous stirring during 20 min. The original dark brown mixture evolved into a black-grayish dispersion. The final mixture was cooled down to room temperature. The black solid was isolated from the liquid media by centrifugation. The product was purified with successive washings of ~3 × 15 mL of acetone, ~3 × 15 mL of water, and ~3 × 15 mL of acetone. Finally, the composite was dried in a vacuum oven at 120 °C during three days.

2.5. Synthesis of Bi_2S_3

The synthesis procedure is the same route used to obtain the composites Bi_2S_3@GO. Briefly, a 5×10^{-3} M dimethylsulfoxide (DMSO) solution of bismuth nitrate pentahydrate (121.27 mg, 0.25 mmol) was prepared. In another flask, 20 mL of DMSO were heated up to 110 ± 2 °C and, once this temperature was reached, it was added 64.12 mg (0.25 mmol) of elemental sulfur. Once the entire yellow solid was dissolved, the Bi^{3+} solution was slowly poured into the sulfur solution. The new mixture was allowed to reach 110 ± 2 °C; then it was added 5 mL of a concentrated solution of ammonium hydroxide (28.3% NH_3) and left under heating and stirring during 20 min. The final mixture was cooled down to room temperature. The black solid was isolated from the liquid media by centrifugation. The product was purified with successive washings of ~15 × 3 mL of acetone, ~15 × 3 mL of water, and ~15 × 3 mL of acetone. Finally, the composite was dried in an oven at 120 °C during three days.

3. Results and discussion

3.1. Synthesis of graphene oxide (GO)

Once the graphene oxide (GO), a dark brown solid, was obtained and purified, it was characterized and compared with its precursor species, the pyrolytic graphite, with the objective to analyze the changes taken place in the spectra profiles, diffractograms and micrographs of the product.

From the structural point of view, the pyrolytic graphite used as precursor presented a diffractogram that corresponds to the one informed in the card (PDF No.41–1487), shown in Fig. S1 a. Pure pyrolytic graphite has an hexagonal crystal system with a space group $P6_3/mmc$ and cell parameters a = 5.195 Å, b = 11.701 Å, c = 5.092 Å, and β = 90.379°. The diffractogram from the graphite precursor exhibited just one intense diffraction peak at 2θ = 26.5° corresponding to {0 0 2} family planes and an interlayer graphite distance of 3.4 Å. In contrast, once the graphite has undergone the Hummer's process [35] aimed to synthesize graphene oxide (GO), the diffraction peak at 2θ = 26.5° broadened and its intensity decreased. Further still, the effective exfoliation of the tridimensional assembly in the graphite structure was confirmed by the appearance of a new, intense, and broad peak at 2θ = 12.1°, which indicated an interlayer spacing increment from 3.35 Å to 7.35 Å [36–39], as shown in Fig. S.1.b. Nonetheless, the remaining broad and minor diffraction peak around 2θ = 25.5° was associated with the existence of a minor fraction of the product that remained as stacked non-oxidized graphene. These still stacked layers were exfoliated when the product was treated with an ultrasound bath during 3–4 h.

Dispersion Raman analysis of the dark brown solid and the precursor raised similar results. Raman spectrum of graphite, shown in Fig. S.2 a, exhibited two distinct peaks at 1582 cm^{-1} and 1314 cm^{-1}, labeled as *G* and *D*, respectively [40–42]. The G band was associated with the doubly degenerated (transversal and longitudinal optical) phonon mode with an E_{2g} symmetry at the Brillouin zone [40]. In pristine graphite the signal at ~1350 cm^{-1} called *D* band should not appear, since it is originated from a double resonance Raman process that it is only permitted in a disordered defected graphite structure [40]. Yet it was possible to detect it in our initial graphite precursor at 1314 cm^{-1}, which indicates the presence of defects in the reagent. Nonetheless, this should not represent a problem in further process.

Once the graphene oxide was obtained (Fig. S.2 b), the *D* band, now centered at 1311 cm^{-1}, grew, widened and shifted to lower wavenumbers indicating an additional disordering in the AB stacking tridimensional graphite structure. This result can be explained as an effective exfoliation of the graphitic AB order into graphene, alongside an increasing oxidation level of the structural aromatic hexagonal rings, which help to further exfoliate the AB layers [36,43]. Accordingly, the original *G* signal widened, as can be seen in Fig. S.2 *b*. From this experimental peak, we were able to deconvolute two new bands at 1606 cm^{-1} and 1517 cm^{-1}, in addition to the original band at 1583 cm^{-1}. The first signal, at higher wavenumbers resembles the *D'* band, informed to appear when extensive structural disorder in graphene oxide is present in its structure [36]; further still, the appearance of the second band, at 1517 cm^{-1}, might indicate changes in the strain of the aromatic rings, presumably due to graphene oxide layers folding [40].

The electronic absorption spectrum using diffuse reflectance mode

showed only an intense band centered around 270 nm (Fig. S.3) that can be assigned to π→π* transition in C=C remaining bonds in graphene oxide structure [44]. The presence of a shoulder near 300 nm indicated a minor existence of C=O bonds, since a n→π* transition is informed [45] when high concentrations of carbonyl bonds were formed during oxidation process.

Even further, the correspondent Tauc plot with a linear extrapolation to determine a band gap value of 4.02 eV is shown in the inset in Fig. S.3. This energy value can be associated with a highly oxidized graphene oxide specie, as a result of the extensive oxidation times employed in the present investigation, this is in agreement with previous reports in the literature [43,45].

XPS was used to study the surface chemical structure. Initially, a survey spectrum was acquired to determine an elemental analysis over the GO sample. The results are displayed in Fig. 1 a where only peaks assigned to C and O could be detected undoubtedly. An additional small peak associated to S was identified, probably as a result of an insignificant contamination due to sulfuric acid used to oxidize and exfoliate graphene sheets. These types of contaminants have been detected in previous studies [37].

Then, high-resolution spectra in the C 1s and O 1s zones were achieved in order to determine the functional groups present in the GO surface. In the C 1s zone of the spectrum of the graphene oxide, four bands could be deconvoluted from the original C 1s spectrum (black dotted line, Fig. 1 b) to obtain the fitted spectrum in red. The first peak at 284.48 eV, blue line, was located at lower bind energy and could be associated to less oxidized species, thus it was assigned to C−C and C=C sp^2 carbons belonging to the residual aromatic graphene structure [46,47]. The signal at 284.80 eV, in pink, is the typical band associated to C−C sp^3 carbons in every XPS analysis performed, consequently here it was related to sp^3 carbons in the newly formed graphene oxide structure [43,46,48]. The band at 286.97 eV, in green, could be associated to alcohol species. However, since alcohol functional groups tend to appear between 286.3 and 286.6 eV [49,50] and our band appeared at higher binding energies, it was proposed that the species present in the graphene oxide were probably in the form of alcoxi– anionic species [50–52]. Finally, the peak at 289.01 eV in orange, was fitted to a highly oxidized specie which was subsequently assigned to C=O carboxylic carbon functional groups [48,51]. It was not detected a band associated to epoxide functional group, a very common specie detected in graphene oxide samples synthesized by Hummer's method. Although it is possible that the specie could not be distinguished from the alcohol-species, as has been previously reported in other works [53].

The spectrum obtained in the O 1s zone (shown in Fig. 1 c), confirmed previous results, since it was possible to deconvolute three distinct peaks from experimental results (black dotted line) to obtain the fitted spectrum labeled in red: The first signal, at 531.55 eV in blue, has the lower binding energy, thus it was associated to the least oxidized specie, in this case it was undoubtedly related to carbonyl oxygen [54] from carboxylic functional groups formerly detected from C 1s spectrum; the second deconvoluted peak at 532.8 eV (in orange) was assigned as −OH in previous works [52], thus it is reasonable to assume this signal arises from alcoholic oxygen and probably carbon single-bonded carboxylic oxygen; finally, the band at higher binding energy (535.11 eV, in blue) was assigned to −OH present in water [55]. The last result is in agreement to previous studies where the authors determined the existence of water between the graphene oxide sheets [37,38,56].

TEM analysis of the resulting graphene oxide (GO) product showed long and wide carbon sheets of hundreds of nanometers and very few stacked layers, which are scarcely seen in the micrographs (Fig. S.4 a).

Although the presence of extensive layers of graphene oxide were not evident in most parts of the micrographs, since carbon coats do not tend to present enough contrast in TEM studies, fast Fourier transform (FFT) were carried out on different parts of the background of the micrographs, where a slightly textured contrast is observed, as the one

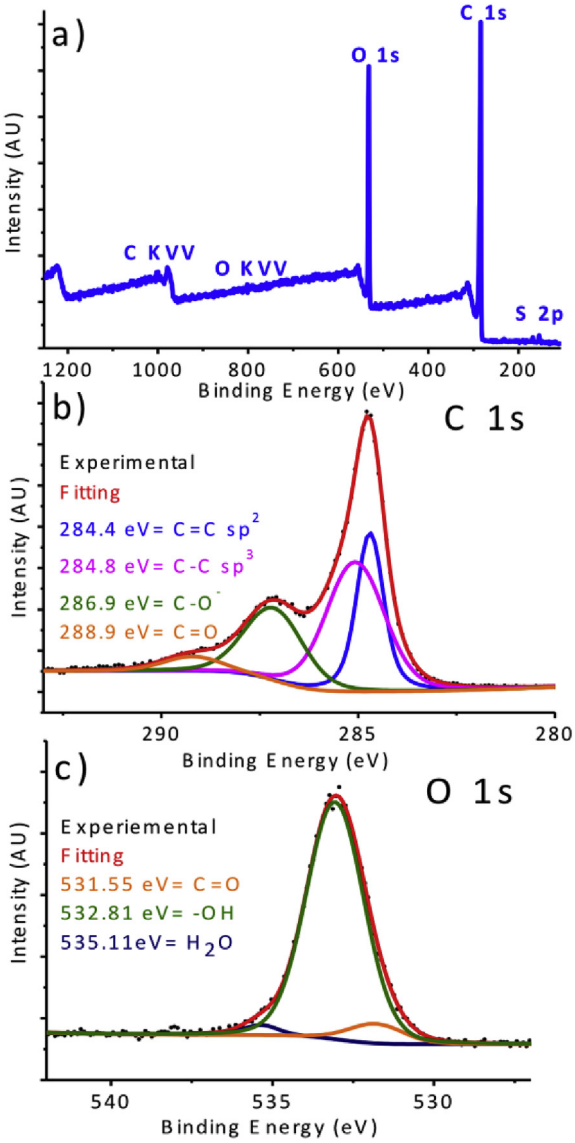

Fig. 1. XPS analyses on a GO sample: (a) Survey spectrum, on the sample, where it was possible detect the elements C, S and small quantities of S; (b) High-resolution spectrum on the C 1s band and on (c) O 1s band, where C=C sp^2, C–C sp^3, −C−OH, C=O, and H_2O species were detected.

showed in Fig. 2 b. In the case of Fig. 2 *a*, from the magenta square region, it was possible to detect a dim hexagonal spot pattern with a mean distance of 2.0 Å (Fig.e 2 b). The spots in the hexagonal arrangement correspond with {1 0 1} family planes in graphene oxide, and they match with the six-fold crystal symmetry of original graphene layers [57], which is still present in the graphene oxide obtained despite the oxidation process fulfilled. Additionally, a couple of spots at a distance of 1.6 Å that match with {1 0 3} family planes were found.

The reconstructed inverse fast Fourier Transform (IFFT) was performed; therefore the image shown in Fig. 2 c could be drawn. This image showed clearly the honeycomb hexagonal arrangement of carbon representative of graphene layers, which can be seen in the red inset in Fig. 2c, from the red area. It is noteworthy that this organization was not discernible in the original micrograph (Fig. 2 a), yet once the reconstructed IFFT was performed the typical carbon framework was certainly detected. All the magenta squared area seemed to be covered by a coating of graphene oxide composed of few layers. With this assay, it was possible to undoubtedly identify the presence of graphene films covering different surfaces. It is important to mention that graphene

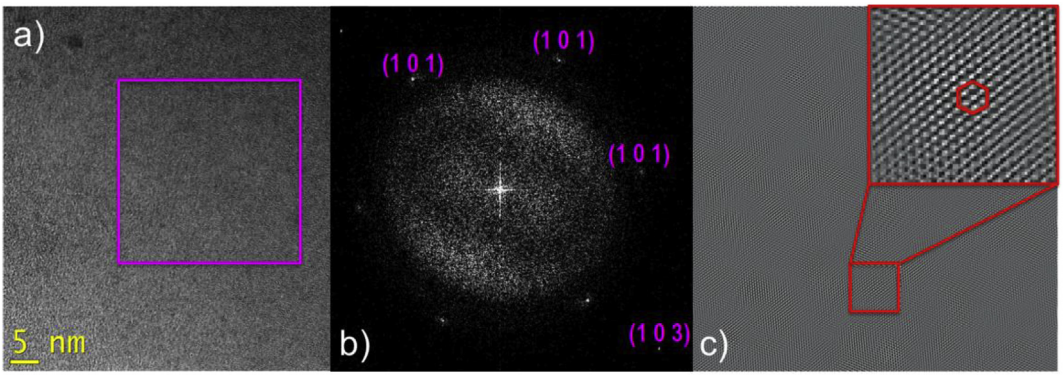

Fig. 2. High-resolution transmission electron micrograph (HR-TEM) of synthesized graphene oxide (GO) (a). Even if it was not very evident the presence of GO in the micrograph (a), once a fast Fourier transform (FFT) pattern was performed at the magenta square region, a spot pattern corresponding to a few sheets of GO was detected (b).

and graphene oxide patterns, similar to the ones we identified, were already informed in other works [57–59]. The possibility to detect thin graphene oxide sheets by FFT-TEM analysis gave us a powerful tool to identify graphene oxide on bismuth sulfide surfaces.

Subsequently, Fig. S.4 b show a SEM image obtained with secondary electrons for a GO sample, where smooth surfaces could be detected. When energy-dispersive X-Ray spectroscopy analysis on the sample was performed, C and O were the main elements detected in accordance with XPS survey analysis performed previously. Small quantities of S were also detected (less than 2%), probably due to the media used to synthesize GO.

Finally, to evaluate the possibility of constructing Bi_2S_3@GO composites, the surface potential of a sample of 6.5 mg of GO was determined. The dark solid was exfoliated and suspended in 13 mL of deionized water and exfoliated by sonication. Then, the GO dispersion was analyzed with a particle charge detector (Mütek) [60]. The dispersion was titrated with the cationic polyelectrolyte poly(dimethyl diallyl)ammonium chloride. The resulting surface potential value was −51.06 C/g. This cypher means that the surface of graphene oxide has a net negative charge, which agrees with the result obtained by XPS about the partial deprotonation of −OH functional groups and existence of alcoxi-anionic ($-O^-$) species on the GO structure. This information allowed us to establish an experimental condition, the previous mixing of bismuth salt cation (Bi^{3+}) and the exfoliated GO, in order to favor the coordination/impregnation of graphene with the Bi^{3+} precursor and the successful synthesis of Bi_2S_3-GO composites.

All analysis techniques supported the positive synthesis of well-exfoliated graphene oxide sheets with a high-level of oxidation. One of the most important methods to detect the GO layers was HR-TEM analysis; since the employment of reconstructed IFFT analyses allowed us to reveal thin coatings of GO in places where they were not clearly visible by direct visualization on the graphene oxide micrographs. Additionally, according to XPS studies GO sheets had attached −OH and −OOH functional groups to their C−C skeleton structure. Small quantities of water were detected, an expected result according other studies [37,38,56]. The negative surface potential determined agrees with the XPS interpretation related with the possible existence of partially ionized methoxy groups ($C-O^-$) in the graphene oxide structure, which would result in an advantage for the fortunate composite preparation.

3.2. Synthesis of Bi_2S_3@GO composites

Dimethylsulfoxide was used as solvent in the Bi_2S_3@GO composite synthesis due to the better solubility of bismuth nitrate in DMSO than water and to avoid formation of $(BiO)_2CO_3$, a typical by-product when Bi^{3+} ion is kept in water in presence of ambient CO_2 [13].

Additionally, elemental sulfur was used instead of sodium sulfide (Na_2S) since it was previously reported by our group that Na^+ presence leads to formation of mixed sodium-bismuth sulfide ($NaBiS_2$) [19].

According to literature [61,62], elemental sulfur (S_8) tends to undergo a disproportion reaction in presence of hydroxide species (OH^-), as shown in equation (1). The main products formed during the reaction are thiosulfate ($S_2O_3^{2-}$) and polysulfides species (S_3^{2-} and S_2^{2-}). The later species tend form sulfide ions (S^{2-}), according to equations (2) and (3). With these reactions, it was possible to avoid by-products such as $NaBiS_2$ and it made it possible to feed the reaction media with enough sulfide ions to form the pure product (Bi_2S_3).

$$S_8 + 6OH^- \rightarrow 2S_3^{2-} + S_2O_3^{2-} + 3H_2O \quad (1)$$

$$S_2^{2-} + 2e^- \rightarrow 2S^{2-} \quad (2)$$

$$S_3^{2-} + 4e^- \rightarrow 3S^{2-} \quad (3)$$

Once the Bi_2S_3@GO composite was obtained, the first analysis performed to the clean sample was Raman dispersion spectroscopy, which can be shown in Fig. S.5 a.

In previous studies performed by Zhao's et al., the authors calculated 27 Raman-active phonon modes in an orthorhombic Bi_2S_3 cell structure [63], from these calculated signals, they detected experimentally 17 of them. Based on this research, the signals located at 32 cm^{-1}, 53 cm^{-1}, 70 cm^{-1}, 86 cm^{-1}, 173 cm^{-1}, 184 cm^{-1}, 237 cm^{-1}, and 253 cm^{-1} could be matched with the deconvoluted signals from the spectrum acquired for our Bi_2S_3@GO composite at 35 cm^{-1}, 50 cm^{-1}, 69 cm^{-1}, 89 cm^{-1}, 165 cm^{-1}, 183 cm^{-1}, 234 cm^{-1}, and 254 cm^{-1} (Fig. S.5 a). Accordingly, the first, third and fourth peaks can be associated to B_{1g} phonon modes, whilst the rest of them were assigned to A_g phonon modes. There is a slightly difference between the reported values and the ones we determined in our sample, nonetheless the variation may be due to the deconvolution method employed and its limited accuracy. The rest of the signals appeared to be too weak to be detected in our Raman spectrum.

Additionally to the peaks corresponding to Bi_2S_3 component, two small and broad signals centered around 1350 cm^{-1} and 1580 cm^{-1} were detected (*Figure S.5 a*), indicating the presence of graphene oxide in the sample. In this zone, once a deconvolution method was applied, the same bands previously achieved for pure graphene oxide were detected. Hence, this analysis allowed us to suggest the positive existence of Bi_2S_3@GO composite.

In concordance with Zumeta-Dubé et al. no other peaks were detected beyond 300 cm^{-1} in the Bi_2S_3@GO composite sample, using a laser power of 1 W. The absence of other peaks beyond 300 cm^{-1} agreed with the suitability of this synthetic method to obtain pure bismuth sulfide samples, since there are no by-products such as $S_2O_3^{2-}$ or SO_3^{2-} present during the formation step. However, once the laser power was increased, signals arisen above 500 cm^{-1}. In concordance to

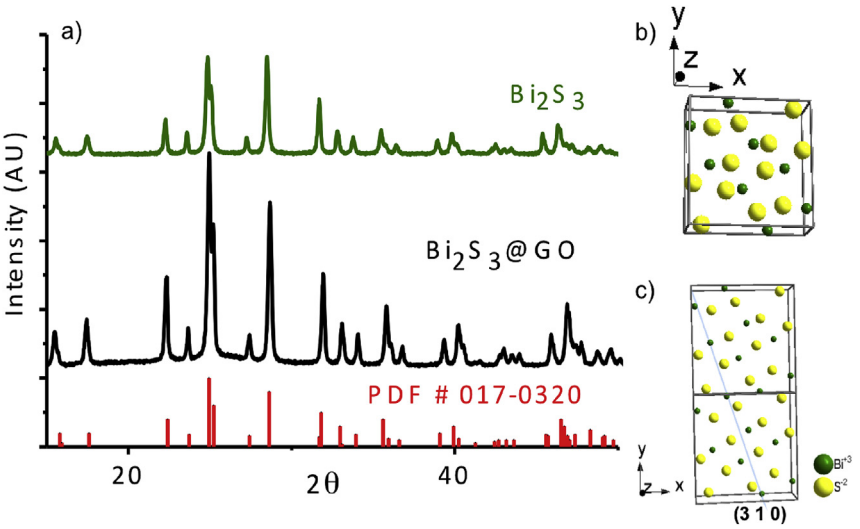

Fig. 3. (a) X-ray diffraction patterns of pure Bi_2S_3 (dark green line) and the Bi_2S_3@GO composite (black line), where it was determined the orthorhombic crystal cell structure obtained (b); the former pattern has a very intense diffraction peak {3 1 0} as a result of a presumably preferential growth along the {3 1 0} plane, as shown in (c). (For interpretation of the references to colour in this figure legend, the reader is referred to the Web version of this article.)

the aforementioned authors, the appearance of these signals would implicate the degradation of bismuth sulfide rods into thiosulfate, sulfate, sulfite and other oxianionic species.

Consistent with the previous assay, in pristine bismuth sulfide particles almost the same bands were deconvoluted form the original Raman spectrum (Fig. S.5 b, dark green spectrum), with an extra band at 227 cm^{-1} (shown in dark blue in Fig. S.5 b), which could be assigned to a B_{3g} phonon mode and it was also present in the research performed by Zhao et al. [63].

Then, XRD analysis was performed in order to undoubtedly determine if Bi_2S_3 was present, as hinted by Raman spectroscopy. The result from pristine Bi_2S_3 sample is exhibited in Fig. 3 a, dark green line. The diffraction pattern matched perfectly with the powder diffraction file PDF # 17–0320 (pattern in red). All the diffraction peaks corresponded to orthorhombic bismuth sulfide with a space group *Pbnm*; cell parameters a = 11.170 Å, b = 11.319 Å, and c = 3.992 Å; and twenty atoms per unit cell [64], according to the crystal cell displayed in Fig. 3 b. Not other species were detected with this technique.

Further, the diffraction pattern of the Bi_2S_3@GO composite was acquired (Fig. 3 a, pattern in black). Likewise, all the peaks matched with the PDF # 17–0320 card, which means that the bismuth sulfide in the aforementioned composite had the same orthorhombic structure, the same space group, cell parameters, and number of atoms in the unit cell. However, an important difference was detected: the diffraction peak corresponding to {3 1 0} plane family had a higher relative intensity than the intensity reported in the proper PDF card. This elongated peak gave us the first hint about a preferential growth along one direction, presumably along the {3 1 0} plane family, which runs predominantly along the *y* axis and encloses a pile of Bi^{3+} ions, green spheres as shown in Fig. 3 c. This first evidence would be later reinforced by other techniques.

In order to determine if the implied components GO and Bi_2S_3 structures were present as a composite or as a physical mixture, TEM assays were performed. First, low-resolution microscopy assays were implemented to detect the thin fragile GO sheets. The resulting micrographs are displayed in Fig. 4 Images in Fig. 4 a and b show elongated assemblies having diameters of more than 150 nm and lengths of approximately 0.5 μm. This form matched with the previously detected bismuth sulfide preferential growth, presumably along the {3 1 0} family planes, according to XRD analyses (Fig. 3 a, black diffractogram).

Remarkably, in the images, the Bi_2S_3 rods appeared to be surrounded by semitransparent wrinkled layers, which seem to correspond to GO. These films seem to be torn due to the implementation of an ultrasound procedure in order to improve the dispersion of the samples to be better analyzed by TEM technique.

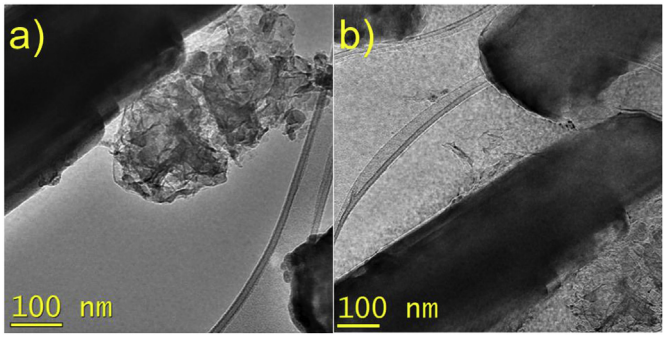

Fig. 4. Low-resolution TEM images (a) and (b) of a Bi_2S_3@GO sample. In every micrograph, elongated structures with approximately 100–150 nm in diameter and 0.5 μm in length were observed. Additionally, all the rods seem to be enclosed in semitransparent layers of what appears to be GO.

Afterwards, high-resolution micrographs were acquired from a Bi_2S_3 rod edge; the results are shown in Fig. 5. From the image presented in Fig. 5 a, it was possible to establish that the bars are very well crystallized structures and they were indeed surrounded by thin and scarcely perceptible layers, like the one barely observable in the magenta square region. In order to establish the identity of both structures, a FFT analysis was performed all along the micrograph. However, the presence of some small crystals on the surface of the rod made difficult the correct examination of the spot pattern obtained, since we obtained overlapped patterns that corresponded to different crystals. For this reason, it was decided to focus on the yellow squared area, where it was possible to acquire a mono crystalline theoretical diffraction pattern that allowed us to study the zone (Zone 1).

The resulting FFT obtained from this Zone 1 is shown in Fig. 5 b. This array consisted of two elements: The most intense points belonged to Bi_2S_3 in the elongated structure. All the intense diffraction spots, which were also piled along the *y* axis, could be matched with the {0 *k* 0}, {1 *k* 1}, and {2 *k* 2} family planes, as indicated in Fig. 5 *b* (Miller indexes labeled in yellow). Furthermore, it was possible to detect a second series of dim spots with a mean distance of 1.6 Å, which could not be indexed to the Bi_2S_3 structure. These faint dots resembled the distances established in the GO layers previously presented in Fig. 2, where two faint points with the same distance were detected. The presence of these spots, which had a multiplet at a mean distance of 0.8 Å, would indicate the presence of sheets of graphene oxide on the surface of the rod (diffraction points with Miller index labeled in magenta). It is worth to mention that this dim dots arrangement appeared not only in this zone, but also in most part of the composite's rods.

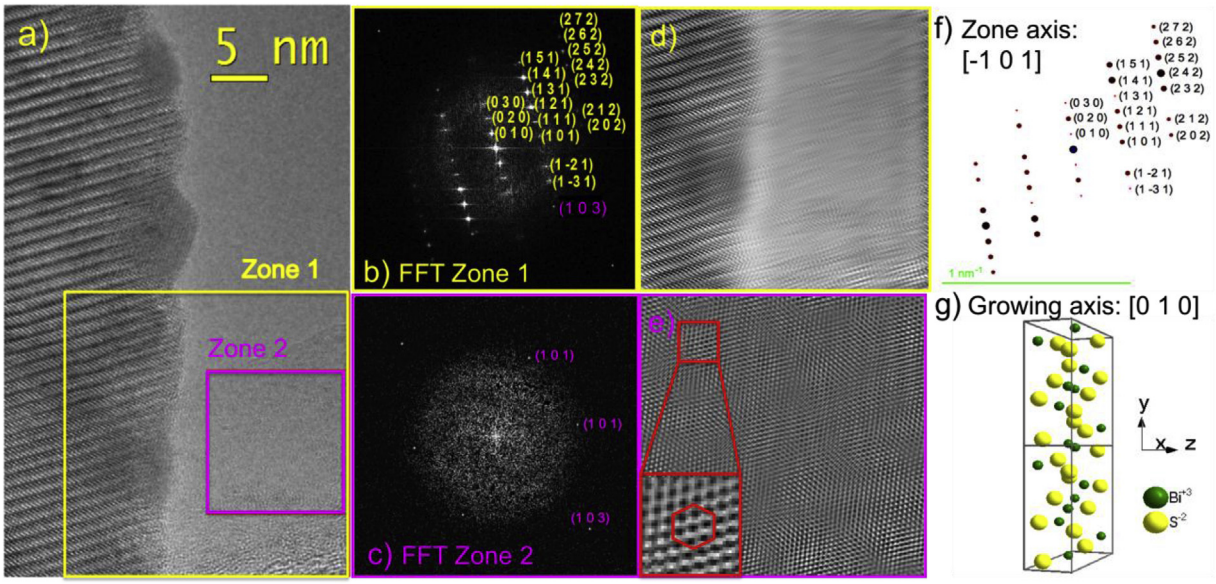

Fig. 5. High-resolution TEM micrograph (a) of a Bi_2S_3 rod edge. The micrograph presents a well-crystallized rod that is surrounded with a thin layer of GO. From zone 1 in (a) an FFT assay was performed in (b) to determine that in the region two components are present: reflections indexed to Bi_2S_3 crystals (Miller indexes in yellow), which formed the IFFT image shown in (d) that reconstruct the edge of the analyzed rod; and dim reflections indexed to GO thin films (Miller index in magenta). The indexing of this spots was confirmed when a FFT assay was performed on Zone 2. This FFT pattern is shown in (c), which was used to reconstruct the image in (e) that reveals the carbon honeycomb hexagonal structure typical in GO. Employing the FFT from the rod edge (Miller indexes in yellow), it was established the zone axis as [−1 0 1] (f), which made possible to calculate the growing axis as [0 1 0] (g). Hence, it was determined that the rod tends to grow along the *y* axis. (For interpretation of the references to colour in this figure legend, the reader is referred to the Web version of this article.)

Nevertheless, this micrograph was chosen since it allowed a better scrutiny of the composite.

With the purpose to verify the identity of the last set of reflections, an additional FFT was performed, but in this occasion, centered at a zone where only GO seems to be present (magenta squared region labeled as Zone 2 in Fig. 5a*)*. This area was selected due to the presence of a thin semi-transparent sheet that resembles the layers previously detected when GO was examined by TEM assays (Fig. 2 a). When the FFT was implemented at the magenta zone, the dots arrangement shown in Fig. 5 c was detected. Four of these spots had a mean distance of 2.0 Å, which could be compared with the reflection dots corresponding to the {1 0 1} diffraction family planes in graphene oxide. The {1 0 1} arrangement resembled the hexagonal pattern obtained for pure GO (Fig. 2 b), but in an incomplete form. Another couple of points, with a mean distance of 1.6 Å, clearly corresponded to the previously detected dim spots in the FFT from the yellow squared region. These reflections corresponded with the {1 0 3} family planes in GO. This assay confirmed undoubtedly the presence of GO in this part of the micrograph.

The former spots, matching the {1 0 1} family planes, do not seem to be present in the FFT design shown in Fig. 5 b, where both Bi_2S_3 and GO reflections are present. However, it was expected that these dots might be hidden by the more intense Bi_2S_3 reflection arrangement.

Further still, using the FFT patterns obtained from the Zone 1 and Zone 2, it was possible to perform the reconstructed IFFT for the two different sets of diffraction patterns present in FFT in Fig. 5 b. First, from the intense spots labeled in yellow, the image shown in Fig. 5 d was reconstructed. In the recreated image, the rod's edge is clearly appreciated. Thus, these reflections unquestionably correspond to the Bi_2S_3 elongated structures.

In contrast, when the FFT pattern in Fig. 5 c, corresponding to GO, was used to perform the IFFT, it was possible to generate the image shown in Fig. 5 e. In this case, the reconstructed image showed a thin coating with hexagonal honeycomb arrangement, as seen in the inset in Fig. 5 e. This film is in concordance with the typical structure of carbon hexagonal pattern, previously detected in graphene oxide layers (Fig. 2 c). Hence, these reflections certainly correspond to the graphene oxide thin layers on top of the rods.

It is important to mention that in order to reconstruct the original micrograph, the spots corresponding to GO in Fig. 5 b were not used, since the diffraction pattern seems to be incomplete due to the mayor intensity of the diffraction dots from bismuth sulfide elongated structures that appear to hide the dim GO diffraction specks. Due to this fact, the performance of a reconstructed IFFT with only the presence of the spots from Fig. 5 b would not create the whole recreated structure, making the assay meaningless.

Another evidence to reinforce the existence of GO on the surface of Bi_2S_3 rods was the employment of the spot arrangement corresponding to Bi_2S_3 rods to calculate the zone axis. This direction was established as: [−1 0 1]. From this direction, it was possible to recreate the exact diffraction pattern shown in Fig. 5 f., which is identical to the original FFT pattern displayed in Fig. 5 b. This constructed diffraction pattern does not exhibit a spot where the GO specks are present (Miller index in magenta).

Furthermore, since the growing axis should be perpendicular to zone axis (the length of the rod runs perpendicular to the axis zone) in the as-synthesized rods, the preferential Bi_2S_3 rod growth would be given in along the [0 1 0] direction, meaning that the unit cells would be piled up one on top of other lengthwise the y axis. This finding is in agreement with previously mentioned tendency of the Bi_2S_3 orthorhombic unit cell and the natural tendency of this structure to grow in infinite chains of Bi and S ions, one on top of other directed along the [0 1 0] axis [3] (in *Pbnm* space group), as seen in Fig. 5 g.

However, if the formation of infinite chains of −Bi− and −S− elements along the *y* axis were the only reason for preparing rod-like structures, and the presence of GO did not affect the formation of these shapes, we would obtain the same elongated arrangements under the same reaction conditions, even if the GO is absent; perhaps we would obtain some variations in length/width ratio.

Therefore, to test the abovementioned suggestion, pristine bismuth sulfide structures were synthesized under the same reaction conditions and concentrations, but without graphene oxide sheets, in order to compare with the composite Bi_2S_3-GO. The result is shown in Fig. 6.

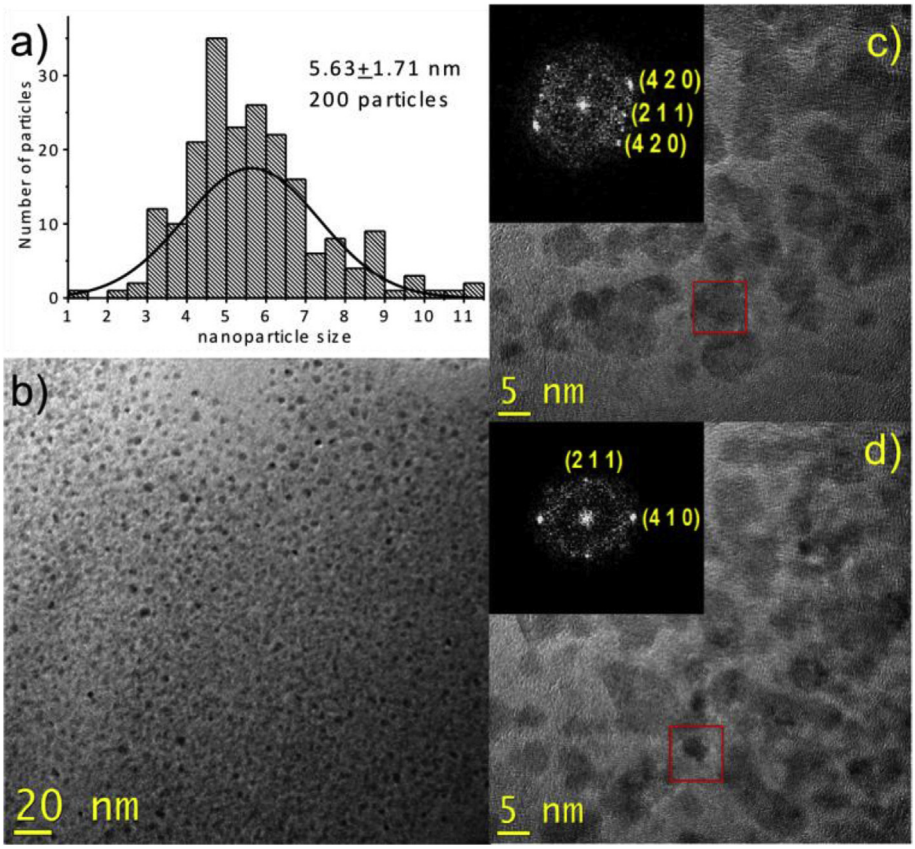

Fig. 6. High-resolution transmission electron images of pure Bi_2S_3 synthesized under the same conditions as the Bi_2S_3@GO composite. Outstandingly, spherical particles partially agglomerated with mean size of 5.6 nm were detected.

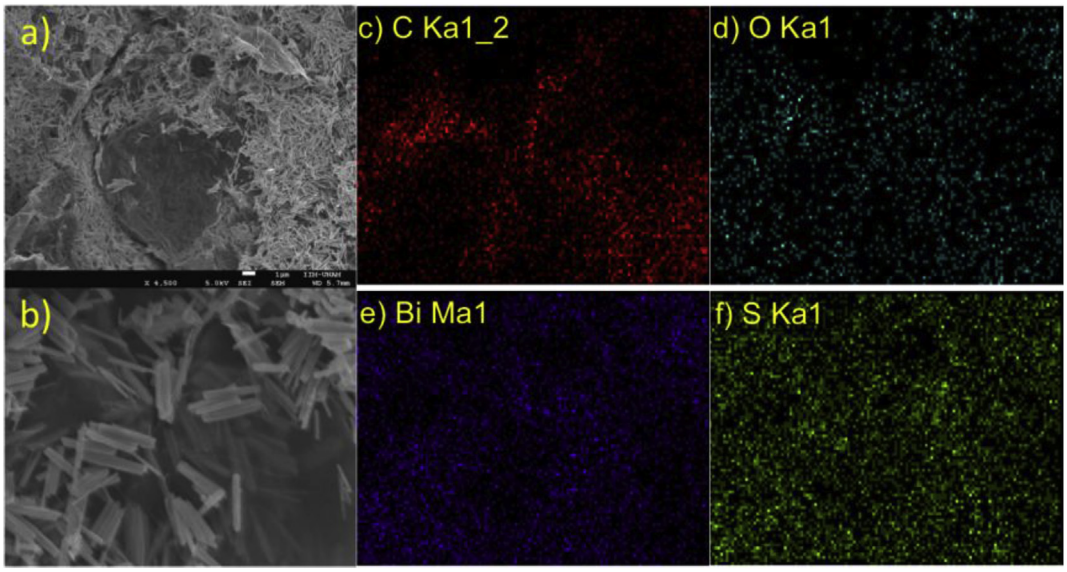

Fig. 7. Scanning electron microscopy studies on the Bi_2S_3@GO composite. Rod-like structures anchored to semitransparent GO sheets are detected throughout the analysis (a) and (b). The EDS analysis revealed the presence of C (c), O (d), Bi (e), and S (f), all the elements present in the composite. In particular the Bi and S elements were detected in the zones corresponding to rod populations, whilst the C and O were located where more semitransparent sheets were placed.

From pure bismuth sulfide TEM micrographs it was possible to detect small spherical crystals with mean size value of 5.6 nm and standard deviation of 1.7 nm (Fig. 6 a). When the FFT was acquired from the selected areas included in the red squares, displayed in Fig. 6 c and Fig. 6 d, it was feasible to obtain the appropriate theoretical electron diffraction patterns of these images (insets in Fig. 6 c and Fig. 6 d).

From these diffraction patterns the identity of the nanocrystals was corroborated, since all of them show diffraction spots corresponding to {2 1 1}, {4 1 0}, and {4 2 0} planes, which match with d = 3.11 Å, d = 2.70 Å, and d = 2.50 Å distances, respectively.

The most relevant result was the detection of spherical particles obtained by the same synthesis procedure, but now in absence of GO. This contrasting discovery strongly suggests that there is a further reason for the formation of bismuth sulfide rods on GO beyond the pile

up of Bi and S elements along the [0 1 0] axis, as mentioned before. Since there are previous studies where scientists analyze the role of stabilizing agent on the formation of elongated structures [1,2,9,16,30,31], and in this research there was not a solvent change (another factor in growth with preferential shape, as we discussed before), we propose that the reason behind the formation of rods in the present investigation was due to a strong GO influence on the formation of the elongated structures achieved. Then, the graphene oxide might cap certain planes, perhaps the {3 1 0} planes family that contains the infinite Bi^{3+} chains, and favor the crystal growth along [0 1 0] axis. This capping effect would elapse through a coordination effect between −OH and C=O functional groups present on the GO surface and Bi^{3+} cations. However we had to prove this claim.

Further scanning electron micrographs (SEM) of the Bi_2S_3@GO composites obtained with secondary electrons, clearly showed extensive populations of rod-shaped Bi_2S_3 particles with sizes between 150 and 200 nm in wide, and hundreds of nanometers in length. These elongated structures were intercalated between sheets of graphene oxide, as shown in Fig. 7a and b. Populations of rods can be detected behind the GO sheets at those micrographs, since the GO layers did not disperse completely the electron beam, thus they were partially transparent. Furthermore, the thinnest rods tend to assemble in parallel, and all the rods seemed to grow parallel to graphene oxide sheets. This regular and parallel anchorage of rods on the graphene oxide layers support the suggestion about GO and Bi^{3+} preferential coordination.

Energy-dispersive X-Ray spectroscopy (EDS) analyses were further performed in order to determine the presence of elements and impurities in the sample. When EDS was applied on a small area (in Fig. 7 b), it was possible to detect the Bi, S, C and O elements. These elements match well with the components of the composite. Moreover, when EDS in mapping mode was acquired (Fig. 7 c, d, e, and f), it was possible to verify the homogeneity in the dispersion of S and Bi elements present along the whole micrograph, according to EDS results, which would suggest a good dispersion of the rods on the graphene oxide sheets, as well as a high purity of the Bi_2S_3 nanorods. Even if on the image there were zones where layers were present, the presence of S and Bi on the mapping analysis reflected the existence of more rods behind the GO leaves. In contrast, the O and C detection was focused on the zones corresponding to graphene sheets (Fig. 7 c and *d*). This mapping supported the claim that the rods were homogeneously dispersed on the graphene oxide matrix.

In order to get a better comparison of the surface chemical composition between Bi_2S_3@GO composites and the pristine Bi_2S_3 NPs and a deeper understanding on the bismuth sulfide-graphene oxide interaction, XPS analyses were performed on samples of both type of species.

The spectra obtained from pristine bismuth sulfide nanoparticles were obtained and are displayed in Fig. 8. The survey spectrum on the sample showed peaks corresponding to C, O, S, and Bi, all the elements composing the pristine Bi_2S_3, as exhibited in Fig. 8 *a*. The first and second signals were not surprising, since XPS analyses are superficial, thus it is possible to detect surface species not always seen by other techniques, usually solvent remaining. This low and superficial existence of the C and O species detected became evident when the area under the bands, related with the concentration of the species, were calculated for the S and Bi species; since for every C count there were 30 counts for Bi (1:30 ratio).

When the sample was analyzed in the C 1s region, it was possible to obtain the experimental spectrum shown in Fig. 8 b (black dotted line), which was deconvoluted giving two signals, at 284.80 eV (pink line) and 285.97 eV (green line). The first peak is attributed to the typical adventitious carbon associated with sp^3 C−C bonds, which can be found in almost every sample analyzed by XPS [43,46,48] and comes from aliphatic carbon sources. The second peak, located at higher binding energy, it was possible to relate it with short chain alcohols, perhaps methanol, typically present in technical acetone used to wash the samples [65], or acetone itself [54]. Both species were found in low concentrations on the surface of the Bi_2S_3 NPs.

Further still, in the O 1s region it was possible to deconvolute three peaks from the experimental spectrum obtained (Fig. 8 c., black dotted line) at 530.10 eV (violet line), 531.49 eV (orange line), and 532.99 eV (green line). The first curve produced by deconvolution at lower binding energy, which was not detected before, could be assigned to Bi−O bonds [66]. It cannot be attributed to Bi_2O_3, since this oxide compound peak appears near 529.5 eV [67], 0.6 eV below the value determined for this band. Hence, we propose that, as determined by Hoste et al., this feature would be associated with an organic/inorganic Bi−O specie. In this instance, it would come from the formation of a bond between bismuth and oxygen species present on the surface of the Bi_2S_3 sample (either acetone or methanol, previously detected). The second peak, at 531.49 eV (orange line), can be attributed to remaining acetone [54,68] at the surface of the sample, as previously detected in C 1s region. Finally, the peak centered at 532.99 eV (green line) corresponds to the deconvolution of the last band, whose value may be attributed to the presence of −OH species on the sample [52].

In the Bi *4f* region (Fig. 8 d), it was possible to deconvolute two doublet peaks from the original experimental spectrum (black dotted line), each with a doublet separation of 5.3 eV (corresponding to Bi $4f_{7/2}$ and $4f_{5/2}$ bands). The first doublet signal at 158.41 eV and 163.71 eV (light green line) was the result of Bi−S bonds in Bi_2S_3 NPs, according to Ettema [24] and Debbies [69]. This result was expected, since the formation of the compound has been determined previously by other techniques. Unexpectedly, an extra doublet signal could be deconvoluted from the experimental spectrum (violet line), which was located at 159.33 eV and 164.63 eV. Taking in account that the doublet appeared at higher binding energies, it must belong to a bismuth specie bonded to a more electronegative element that in our case it was previously hinted as oxygen. Hence, this band may confirm the existence of organic/inorganic Bi−O bonds [70,71], which would be present on the surface of the Bi_2S_3 sample (either acetone or methanol, previously detected). However, the concentration of the Bi−O specie was comparatively low to the Bi−S bonds existence (1:9 counts ratio for Bi−O:Bi−S bonds).

In the same region as Bi *4f* (Fig. 8 d), it was possible to detect a doublet band associated with the S *2p* signal (cyan line), whose sole values at 161.75 eV and 162.85 eV ($2p_{5/2}$ and $2p_{3/2}$ bands), clearly was correlated to S^{2-} specie bonded to −Bi [69].

Then, the XPS spectra of Bi_2S_3@GO composite were recorded. Once again, the elements C, O, S, and Bi elements were detected when the survey spectrum was obtained (Fig. 9 a), just as it happened with pure Bi_2S_3 sample. However, the O and C bands appeared more intense, as a result of the extensive presence of graphene oxide in the composite (1:9 counts ratio for C:Bi elements). Not other element was detected.

Afterwards, the high-resolution XPS spectrum in the C 1s region was obtained (Fig. 9 b), in that case three signals were deconvoluted from the experimental spectrum (black dotted line), three bands were determined. The first band, centered at 284.14 eV (blue line), can be associated to the signal found at 284.47 eV in the initial GO sample, which corresponded to C=C sp^2 functional groups still present in the graphene structure [46,47]. The second band located at 284.80 eV (pink line), once more was correlated to C−C sp^3 bonds [43,46,48] formed after the Hummers oxidation process [35]. These two bands were already present in the pure GO product before the formation of Bi_2S_3@GO composite. However, the third and fourth bands, at 286.06 eV (green line) and 287.99 eV (orange line), were not observed before and might be related to the interaction between the Bi_2S_3 and the GO present in the composite. The signal positioned at 286.06 eV should correspond to −OH alcoholic functional groups, which were detected previously at higher binding energy (286.97 eV) as a result of a ionized $-O^-$ specie. However, in this case the −OH bonds did not seem to be deprotonated and it is possible that these groups may be coordinated to Bi^{3+}, as a result of the lower binding energy determined, compared with the original signal determined for the GO synthesized

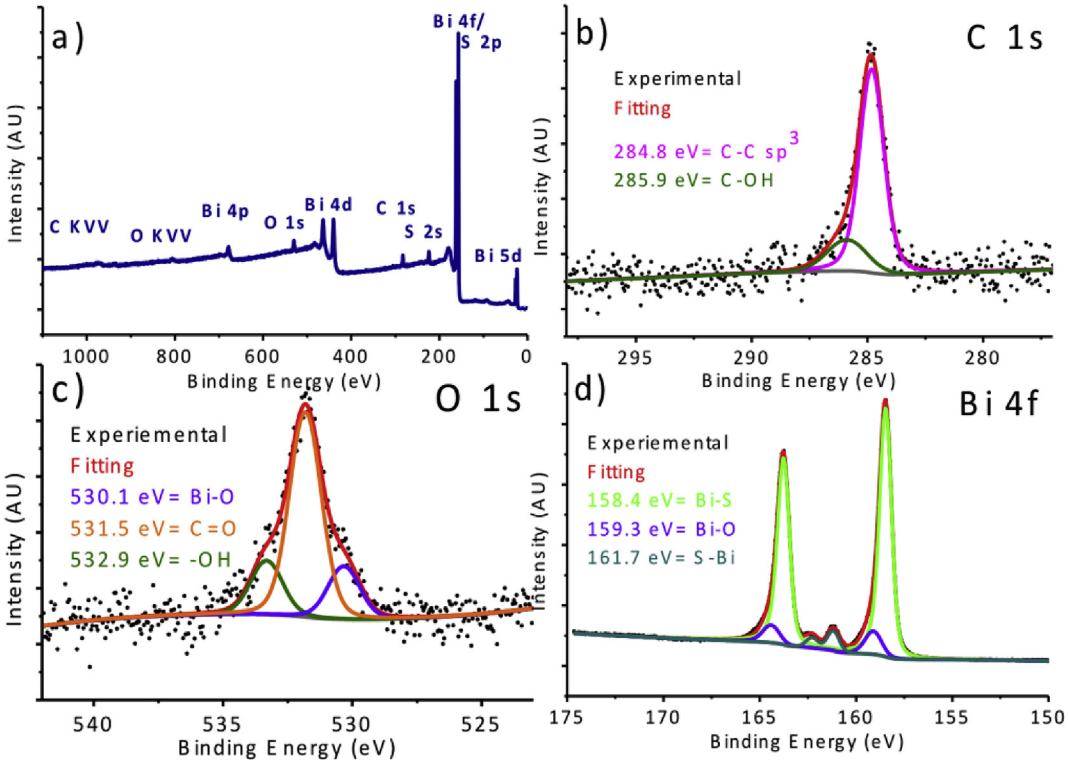

Fig. 8. XPS studies of a pure Bi_2S_3 sample. Survey spectrum (a) and high-resolution analyses on C 1s (b), O 1s (c) and Bi *4f* (d) regions. Aside the detection of Bi—S bonds, the appearance of Bi—O bonds was established.

and the values found in literature for the —OH functional groups [49,50,65,72]. The fourth band, centered at 287.99 eV, according to literature, seemed to correspond to C=O carbonyl groups [48,51], which were once more shifted to lower binding energy when compared to initial GO (288.99 eV). For this reason it is reasonable to assume that these functional groups might be coordinated to Bi^{3+} ions.

On the high-resolution XPS studies on the O 1s region, it was possible to deconvolute three bands from the original experimental

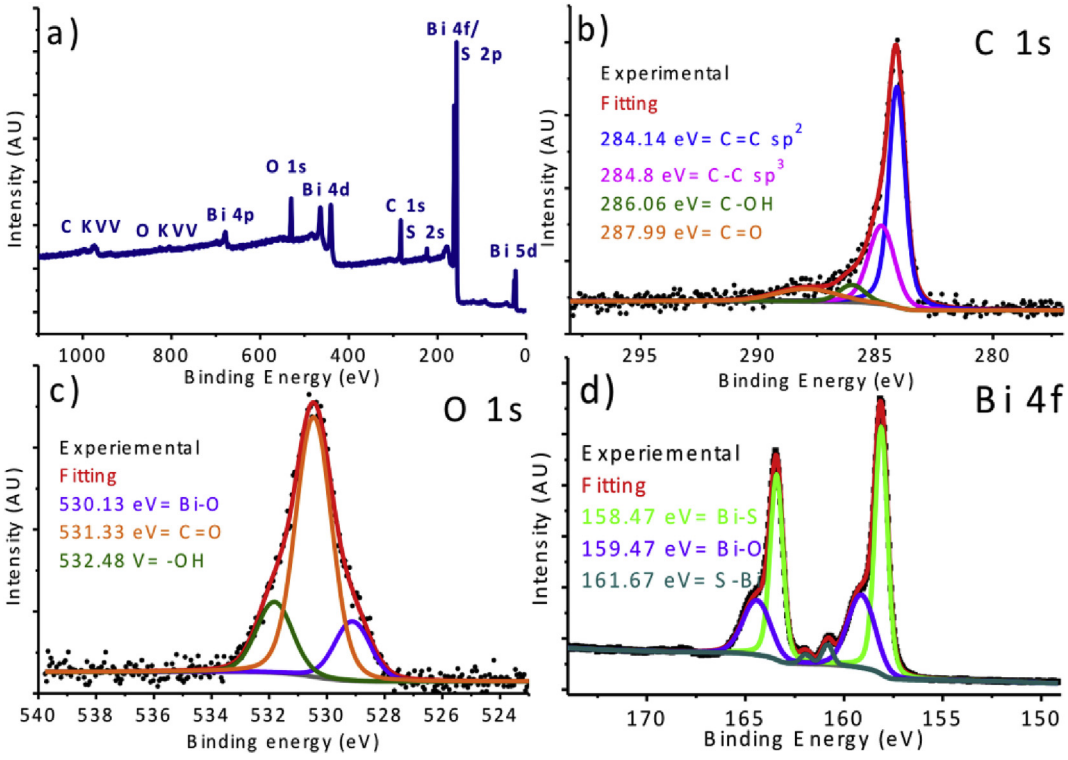

Fig. 9. XPS studies of a Bi_2S_3@GO sample: Survey spectrum (a) and high-resolution analyses on C 1s (b), O 1s (c) and Bi *4f* (d) regions. It was proposed the existence of Bi—O bonds as the responsible for the preferential formation of rod-like structures.

spectrum (Fig. 9 c, black dotted line). The initial band in 530.13 eV (violet line) was again related to the Bi—O specie, and as it was determined by Hoste et al. [66], it belonged to a Bi—O organic/inorganic functional group. This bond would represent a further hint to the importance of these bonds in the formation of Bi_2S_3 rods. The second signal at 531.33 eV (orange line) [54,68] was associated to C=O functional groups from the graphene, as it was previously detected in the pristine GO. Finally, at 532.48 eV (green line), it was located a signal which could be associated to —OH groups [52], once more shifted to lower binding energy than the original band located in the pristine graphene oxide (532.81 eV). Hence, it is feasible to assume a coordination of C—OH groups to the surface of the Bi_2S_3 structures. No water was located in the actual structure, since the product was vacuum heated at 120 °C during three days.

The alleged coordination of Bi^{3+} cations with oxygen functional groups was corroborated by high-resolution XPS analysis in the Bi *4f* zone, since two distinct species were detected, as shown in Fig. 9 d. The first doublet band was situated at 158.47 eV and 163.77 eV (light green line), corresponding to Bi—S bonds present in Bi_2S_3 [24,69]. Additionally, at higher binding energy it was located another more intense doublet band at 159.47 eV and 164.77 eV (violet line), meaning the existence of a specie more oxidized than Bi_2S_3 compound, alleged the presence of Bi—O bonds [70,71,73]. Thus, this band would confirm the existence of organic/inorganic Bi—O bonds in the sample [70,71], as seen in the pure bismuth sulfide sample. However, the existence of these species was far more extensive (2:3 counts ratio for Bi—O:Bi—S bonds) than the one observed in the pristine Bi_2S_3, where its presence seemed to be only as the result of remaining solvent on the surface of the sample. As a result of this noteworthy presence, we propose that, this Bi—O bond has an important role in the preferential formation of rod-like particles in the Bi_2S_3@GO composite. The Bi^{3+} ions in the Bi_2S_3 tend to be aligned along the {3 1 0} family planes in the Bi_2S_3 crystalline structure (as seen in Fig. 3 c). The favored formation of the Bi—O bonds using the oxygen functional groups present in the graphene oxide are most likely responsible for the preferential growth of the Bi_2S_3 rods lengthwise the *y*-axis as represented in Fig. 10. This proposal would explain the different results obtained when the Bi_2S_3 was synthesized underneath the same reaction conditions in presence and absence of the graphene oxide.

Finally, once more in the same Bi *4f* region in Fig. 9 d there was located an extra doublet band at 161.67 eV and 162.77 (cyan line), with a splitting of 1.1 eV, which corresponded to S^{2-} bonded to Bi^{3+}, as determined by Debbies et al. [69]. With this extra signal it was confirmed the presence of Bi_2S_3 in the sample.

As a final analysis pure Bi_2S_3 and Bi_2S_3@GO composite were analyzed by electron absorption spectroscopy in diffuse reflectance mode in order to determine the experimental band gap. Although Bi_2S_3 material has been experimentally evaluated as a direct band gap semiconductor [6,18,23], theoretical studies point out that this material posses a large number of bands [64], whose the smallest of them is an indirect band gap with a value among the 1.2–1.4 eV, depending on the different theoretical methods and calculation accuracy [64,74–77]. A very near direct band gap was also determined [75], at 1.54 eV according to Koc et al. [76]. This theoretical circumstance, linked to the alleged dissimilar structural nature of the samples obtained as a result of the diverse methods of synthesis employed, tend to make difficult to determine the real nature of the band gaps obtained for bismuth sulfide systems [76]. Taking into account this information, it was determinate that the band gaps for our products as both direct and indirect gaps.

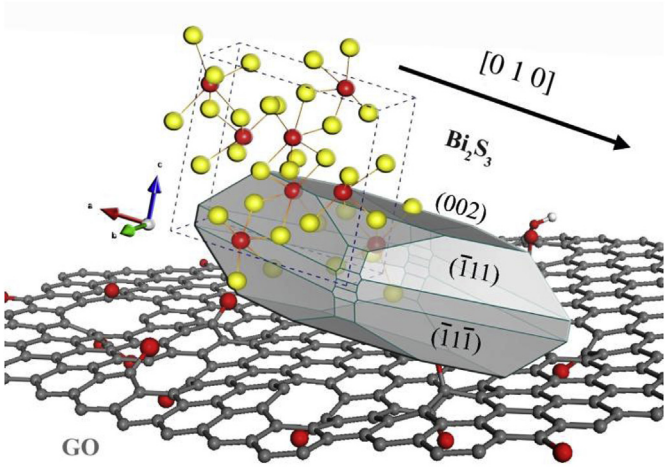

Fig. 10. Representation of a B_2S_3 crystal rod growing parallel to the graphene oxide matrix as a consequence of the formation of Bi—O bonds.

Initially, a sample of pure bismuth sulfur was analyzed and the experimental spectrum is shown in Fig. 11 a, where a broad band, from 200 nm to 900 nm, was recorded. From these data, the Tauc plot was drawn assuming the existence of a direct band gap, $(F(R)*E)^2$. With this new graphic, it was determined a lineal section, which was used to calculate a direct band gap value of 1.36 eV for the pristine Bi_2S_3 (Fig. 11 b). This cipher is concordance with the experimental data reported [6,18,23]. Although it was evident that the mean size (5.6 nm) obtained for the nano-crystalline Bi_2S_3 particles are not small enough to be able to detect a real quantum confinement effect in the pristine Bi_2S_3 NPs sample [19].

Additionally, it was obtained the Tauc plot corresponding to an indirect band gap ($(F(R)*E)^{1/2}$), as seen in Fig. 11 c. From this graphic, it was also located a very clear lineal segment (red line in Fig. 10 c), which was used to determine an indirect gap at 1.08 eV. This result would support the findings made by theoretical studies [64,74–77], where the authors claim the existence of an indirect gap at slightly smaller values than the direct gap, which was usually determined in experimental studies. Although, in our case the quantities obtained were smaller than the calculated ones. Nevertheless, this may respond to the different theoretical methods used and calculation level, as mentioned by Zhan et al. [76].

Then, the Bi_2S_3@GO composite was analyzed with the same technique. The obtained spectrum is shown in Fig. 11 d. Using this data, the Tauc plot for a direct band gap was performed ($(F(R)*E)^2$), where it was possible to determine a lineal portion (red line in Fig. 11 e), which was used to calculate a value of 1.34 eV for the Bi_2S_3@GO powder sample. This numeral is practically the same as the one calculated for pristine Bi_2S_3. The aforementioned result would imply that neither pristine Bi_2S_3 nor Bi_2S_3@GO composite present a quantum confinement effect. In the last case, the reason is evident when the SEM micrographs are reviewed.

In contrast, when the Tauc plot was drawn for an indirect band gap, the presence of a lineal segment was not clearly present, as seen in Fig. 11 f. If this region were indeed present, the calculated value for this indirect band gap would be 1.23 eV, a bigger difference than the one calculated for pristine bismuth sulfide. The clear appearance of this gap is hindered by a presumable dispersion effect in the near-infrared region.

4. Conclusions

A successful synthesis of bismuth sulfide-graphene oxide composites (Bi_2S_3@GO) has been reported. The characterization techniques provided enough evidence about the achievement of pure, well-structured, rod-shaped Bi_2S_3 particles with diameters of more than 150 nm and hundreds of nanometers in length, which are anchored parallel to graphene oxide matrix, and with a direct band gap of 1.34 eV. These elongated structures tended to grow along the *y* axis, according to XRD and HR-TEM analysis. Noteworthy, according to the HR-TEM analyses, the rod assemblies seem to be enclosed in graphene oxide layers, which were detected on the Bi_2S_3 bars surface by FFT and IFFT assays. In

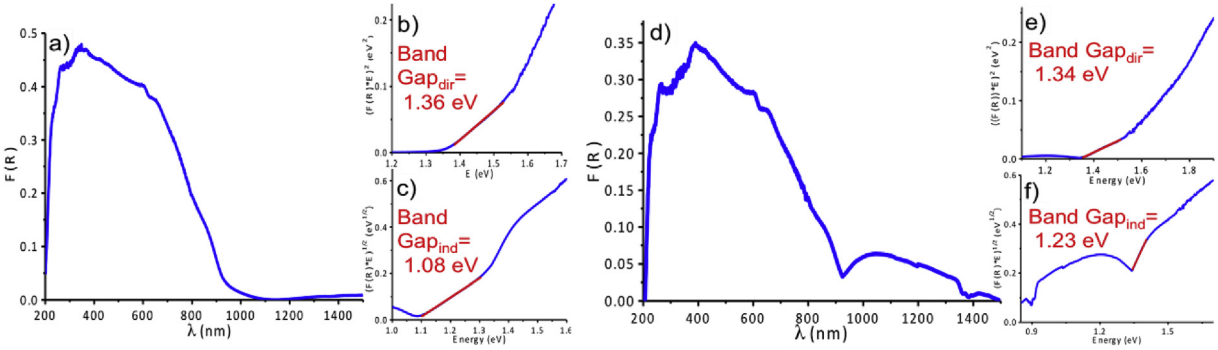

Fig. 11. Absorption electron spectrum of pristine Bi_2S_3 (a) and Bi_2S_3@GO composite (d). And Tauc plots of both spectra. From spectrum of pristine Bi2S3 (a), two very clear band gaps are evident, a direct gap (b) at 1.36 eV, and an indirect gap (c) at 1.08 eV. In constrast, when Bi_2S_3@GO composite spectrum (d) was analyzed, only a direct band gap was clearly present in the Tauc graphics developed (e) with a value of 1.34 eV.

further XPS studies, it was proposed the crucial presence of graphene oxide in the formation of the rod-like structures, due to the occurrence of O—Bi bonds between the Bi^{3+} ions in the rod-like structures, which run in infinite chains along the aforementioned axis, and the oxygen species in GO (—HO functional groups). These Bi—O bonds formations seemed to direct the preferential growth along the [0 1 0] axis, since it was determined that the sole concentration of the precursors was not sufficient to form the elongated particles. Then, consistent and solid evidence was provided by XPS and HR-TEM images, related to the formation of elongated nanostructures of Bi2S3 promoted by GO envelopes.

As a significant by-product, the present research was able to prove the presence of an indirect bang gap in pristine Bi_2S_3, a result predicted by theoretical calculations.

Acknowledgements

García-Peña is grateful with DGAPA-UNAM for the postdoctoral fellowship granted. The authors want to express their gratitude to FQ-UNAM and CONACyT, for the financial support through PAIP 5000-9039, SEPCB-132094 and 2015 CONACyT–SEP basic research project No. 257931. We acknowledge Dr. Patricia Santiago-Jacinto (*Instituto de Física-UNAM* and *Centro de Nanociencias y Micro y Nanotecnología-IPN*), Luis Rendón (*Instituto de Física-UNAM* and *Centro de Nanociencias y Micro y Nanotecnología-IPN*), and Iván Puente-Lee (*USAI Facultad de Química-UNAM*) for facilities granted during TEM experiments; and Cristina Zorrilla, (*Instituto de Física-UNAM*) for Raman analyses performed.

Appendix A. Supplementary data

Supplementary data related to this article can be found at https://doi.org/10.1016/j.matchemphys.2018.08.052.

References

[1] Jiarui Jin, He Tao, Facile synthesis of Bi_2S_3 nanoribbons for photocatalytic reduction of CO_2 into CH_3OH, Appl. Surf. Sci. 394 (2017) 364–370, https://doi.org/10.1016/j.apsusc.2016.10.118.

[2] Shuxi Zhou, Jianmin Li, Yanxiong Ke, Shemin Lu, Synthesis of bismuth sulfide nanorods in acidic media at room temperature, Mater. Lett. 57 (2003) 2602–2605, https://doi.org/10.1016/S0167-577X(02)01334-4.

[3] Kanishka Biswas, Li-Dong Zhao, G. Mercouri, Kanatzidis, Tellurium-free thermoelectric: the anisotropic n-type semiconductor Bi_2S_3, Adv. Energy Mater. 2 (2012) 634–638, https://doi.org/10.1002/aenm.201100775.

[4] S. Vadivel, A. Nirmalesh Naveen, V.P. Kamalakannan, P. Cao, N. Balasubramanian, Facile large scale synthesis of Bi_2S_3 nano rods-grapene composite for photocatalytic photoelectrochemical and supercapacitor application, Appl. Surf. Sci. 351 (2015) 635–645, https://doi.org/10.1016/j.apsusc.2015.04.101.

[5] Shuhong Yu, Yitai Qian, Lei Shu, Yi Xie, Li Yang, Changsui Wang, Solvent thermal synthesis and characterization of ultrafine powder of bismuth sulfide, Mater. Lett. 35 (1998) 116–119, https://doi.org/10.1016/S0167-577X(97)00229-2.

[6] Helal Ahmed, Farid A. Harraz, Adel A. Ismail, Tarek M. Sami, I.A. Ibrahim, Controlled synthesis of bismuth sulfide nanorods by hydrothermal method and their photocatalytic activity, Mater. Des. 102 (2016) 202–212, https://doi.org/10.1016/j.matdes.2016.04.043.

[7] Ya Liu, Yidan Shi, Xiang Liu, Hexing Li, A facile solvothermal approach of novel Bi_2S_3/TiO_2/RGO composites with excellent visible light degradation activity for methylene blue, Appl. Surf. Sci. 396 (2017) 58–66, https://doi.org/10.1016/j.apsusc.2016.11.028.

[8] Subramanian Balachandran, Meenakshisundaram Swaminathan, The simple, template free synthesis of a Bi_2S_3-ZnO heterostructure and its superior photocatalytic activity under UV-A light, Dalton Trans. 42 (2013) 5338–5347, https://doi.org/10.1039/c3dt33117b.

[9] Yajie Chen, Guohui Tian, Guijie Mao, Rong Li, Yuting Xiao, Taoran Han, Facile synthesis of well-dispersed Bi_2S_3 nanoparticles on reduced graphene oxide and enhanced photocatalytic activity, Appl. Surf. Sci. 378 (2016) 231–238, https://doi.org/10.1016/j.apsusc.2016.03.194.

[10] Juan Lu, Qiaofeng Han, Xujie Yang, Lude Lu, Xin Wang, Preparation fo Bi_2S_3 nanorods via a hydrothermal approach, Mater. Lett. 61 (2007) 3425–3428, https://doi.org/10.1016/j.matlet.2006.11.097.

[11] Zhian Zhang, Chengkun Zhou, Lei Huang, Xiwen Wang, Yaohui Qu, Yanqing Lai, Jie Li, Synthesis of bismuth sulfide/reduced graphente oxide composites and their electrochemical properties for lithium ion batteries, Electrochim. Acta 114 (2013) 88–94, https://doi.org/10.1016/j.electacta.2013.09.174.

[12] Guangdi Nie, Xiaofeng Lu, Junyu Lei, Yang Liu, Ce Wang, Facile and controlled synthesis of bismuth sulfide nanorods-reduced graphene oxide composites with enhanced supercapacitor performance, Electrochim. Acta 154 (2015) 24–30, https://doi.org/10.1016/j.electacta.2014.12.090.

[13] Hong Zhang, Lijiu Wang, Synthesis and characterization of Bi_2S_3 nanorods by solvothermal method in polyol media, Mater. Lett. 61 (2007) 1667–1670, https://doi.org/10.1016/j.matlet.2006.07.095.

[14] Xue-Hong Liao, Hui Wang, Jun-Jie Zhu, Hong-Yuan Chen, Preparation of Bi_2S_3 nanorods by microwave irradiation, Mater. Res. Bull. 36 (2001) 2339–2346, https://doi.org/10.1016/S0025-5408(01)00734-6.

[15] J.M. Zhu, K. Yang, J.J. Zhu, G.B. Ma, X.H. Zhu, S.H. Zhou, Z.G. Liu, The microstructure studies of bismuth sulfide nanorods prepared by sonochemical method, Opt. Mater. 23 (2003) 89–92, https://doi.org/10.1016/S0925-3467(03)00065-X.

[16] Guangjian Xing, Zhenjian Feng, Guanghua Chen, Yao Wang, Xuemei Song, Preparation of different morphologies of nanostructured bismuth sulfide with different methods, Mater. Lett. 57 (2003) 4557–4559, https://doi.org/10.1016/S0167-577X(03)00361-6.

[17] Juan Lu, Qiaofeng Han, Xujie Yang, Lude Lu, Xin Wang, Microwave-assisted synthesis and characterization of 3D flower-like Bi_2S_3 superstructures, Mater. Lett. 61 (2007) 2883–2886, https://doi.org/10.1016/j.matlet.2007.01.071.

[18] Wen-hui Li, Synthesis and characterization of bismuth sulfide nanowires through microwave solvothermal technique, Mater. Lett. 62 (2008) 243–245, https://doi.org/10.1016/j.matlet.2007.05.007.

[19] Inti Zumeta-Dubé, Víctor-Fabián Ruiz-Ruiz, David Díaz, Sandra Rodil-Posadas, Adreas Zeinert, TiO_2 sensitization with Bi_2S_3 quantum dots: the inconvenience of sodium ions in the deposition procedure, J. Phys. Chem. C 118 (2014) 11495–11504, https://doi.org/10.1021/jp411516a.

[20] Inti Zumeta-Dubé, José-Luis Ortiz-Quiñonez, David Díaz, Carlos Trallero-Giner, Víctor-Fabián Ruiz-Ruiz, First order Raman scattering in bulk Bi_2S_3 and quantum dots: reconsidering controversial interpretations, J. Phys. Chem. C 118 (2014) 30244–30252, https://doi.org/10.1021/jp509636n.

[21] Xiao Hong Yang, Xiong Wang, Zude Zhang, Facile solvothermal synthesis of single-crystalline Bi_2S_3 nanorods on a large scale, Mater. Chem. Phys. 95 (2006) 154–157, https://doi.org/10.1016/j.matchemphys.2005.05.035.

[22] Xiao-Ping Shen, Gui Yin, Wen-Li Zhang, Zheng Xu, Synthesis and characterization of Bi_2S_3 faceted nanotube bundles, Solid State Commun. 140 (2006) 116–119, https://doi.org/10.1016/j.ssc.2006.08.022.

[23] R.R. Ahire, B.R. Sankapal, C.D. Lokhande, Preparation and characterization of Bi_2S_3 thin films using modified chemical bath deposition method, Mater. Res. Bull. 36 (2001) 199–210, https://doi.org/10.1016/S0025-5408(01)00509-8.

[24] A.R.H.F. Ettema, C. Haas, An X-ray photoemission spectroscopy study of interlayer

charge transfer in some misfit layer compounds, J. Phys. Condens. Matter 5 (1993), https://doi.org/10.1088/0953-8984/5/23/008 38-17-3826.
[25] Ke Zhang, Yuanyuan Wang, Ping Liu, Wei Li, Chemical fabrication and electrochemical performance of Bi_2S_3-nanorods charged reduced graphene oxide, Mater. Lett. 161 (2015) 774–777, https://doi.org/10.1016/j.matlet.2015.08.101.
[26] Ruixia Dou, Zhen Du, Tao Bao, Xinghua Dong, Xiaopeng Zheng, Miao Yu, Wenyan Yin, Binbin Dong, Liang Yan, Zhanjun Gu, The polyvinylpyrrolidonde functionalized rGO/Bi_2S_3 nanocomposite as near-infrafed light-responsive nanovehicle for chemo-photothermal therapy of cancer, Nanoscale 8 (2016) 11531–11542, https://doi.org/10.1039/c6nr01543c.
[27] Otieno Kevin Okoth, Kai Yan, Yong Liu, Jingdong Zhang, Graphene-doped Bi_2S_3 nanorods as visible-light photoelectrochemical aptasensing platform for sulfadimethoxine detection, Biosens. Bioelectron. 86 (2016) 636–642, https://doi.org/10.1016/j.bios.2016.07.037.
[28] Radha Mukkabla, Melepurath Deepa, Avanish Kumar Srivastava, Enhanced lithium-ion storage capability of a bismuth sulfide/graphene oxide/poly(3,4-ethylenedioxythiophene) composite, ChemPhysChem 16 (2015) 3242–3253, https://doi.org/10.1002/cphc.201500515.
[29] Yan Sun, Qiaofeng Han, Juan Lu, Xujie Yang, Lude Lu, Xin Wang, Preparation fo uniform Bi_2S_3 nanoribbons at low temperature, Mater. Lett. 62 (2008) 3730–3732, https://doi.org/10.1016/j.matlet.2008.04.066.
[30] Xiaodong Zhou, Huaqiang Shi, Bo Zhang, Xun Fu, Kui Jiao, Facile synthesis and electrochemical application of surface-modified Bi_2S_3 urchin-like nano-spheres at room temperature, Mater. Lett. 62 (2008) 3201–3204, https://doi.org/10.1016/j.matlet.2008.02.019.
[31] Xiao-Yong Ma, Lu Liu, Wen-Ling Mo, Huajie Liu, Hui-Zhong Kou, Yuqiu Wang, Surfactant-assisted solvothermal synthesis of Bi_2S_3 nanorods, J. Cryst. Growth 306 (2007) 159–165, https://doi.org/10.1016/j.jcrysgro.2007.03.062.
[32] Junfeng Chao, Shumin Xing, Yanchun Zhao, Suling Gao, Qinghua Song, Lixia Guo, Di Wang, Tingliang Zhang, Bismuth sulfide nanoflakes and nanorods as high performance photodetectors and photoelectrochemical cells, Solid State Sci. 61 (2016) 51–57, https://doi.org/10.1016/j.solidstatesciences.2016.09.002.
[33] Supriya A. Patil, Yeon-Taek Hwang, Vijaykumar V. Jadhav, Kwang Ho Kim, Solution processed growth and photoelectrochemistry of Bi_2S_3 nanorods thin films, J. Photochem. Photobiol., A 332 (2017) 174–181, https://doi.org/10.1016/j.jphotochem.2016.07.037.
[34] Yiqing Chen, Huamin Kou, Jing Jiang, Yong Su, Morphologies of nanostructured bismuth sulfide prepared by different synthesis routes, Mater. Chem. Phys. 82 (2003) 1–4, https://doi.org/10.1016/S0254-0584(03)00229-3.
[35] William S. Hummers Jr., Richard E. Offeman, Preparation of graphite oxide, J. Am. Chem. Soc. 80 (1958) 1339, https://doi.org/10.1021/ja01539a017.
[36] Iluminada Rodrígues-Pastor, Gloria Ramos-Fernandez, Helena Varela-Rizo, Mauricio Terrones, Ignacio Martin-Gullon, Towards the understanding of the graphene oxide structure: how to control the formation of humic- and fulvic-like oxidized debris, Carbon 84 (2015) 299–309, https://doi.org/10.1016/j.carbon.2014.12.027.
[37] Sabina Drewniak, Roksana Muzyka, Agnieska Stolarczyk, Tadeusz Pustelny, Michalina Kotyczka-Moranska, Maciej Setkiewicz, Studies of reduced graphene oxide and graphite oxide in the aspect of their possible application in gas sensors, Sensors 16 (2016) 103, https://doi.org/10.3390/s16010103.
[38] Guilin Shao, Yonggen Lu, Fangfang Wu, Changling Yang, Fanlong Zeng, Qilin Wu, Graphene oxide: the mechanism of oxidation and exfoliation, J. Mater. Sci. 47 (2012) 4400–4409, https://doi.org/10.1007/s10853-012-6294-5.
[39] Hae-Kyung Jeong, Yun Pyo Lee, J. Rob, W.E. Lahaye, Min-Ho Park, Hyeok An Kay, Ick Jun Kim, Cheol-Woong Yang, Chong Yun Park, Rodney S. Ruoff, Young hee lee. Evidence of graphitic AB stacking order of graphite oxides, J. Am. Chem. Soc. 130 (2008) 1362–1366, https://doi.org/10.1021/ja076473o.
[40] L.M. Malard, M.A. Pimenta, G. Dresselhaus, M.S. Dresselhaus, Raman spectroscopy in graphene, Phys. Rep. 473 (2009) 51–87, https://doi.org/10.1016/j.physrep.2009.02.003.
[41] Andrea C. Ferrari, Raman spectroscopy of graphene and graphite: disorder, electron-phonon coupling, doping and nonadiabatic effects, Solid State Commun. 143 (2007) 47–57, https://doi.org/10.1016/j.ssc.2007.03.052.
[42] Yanwu Zhu, Shanthi Murali, Weiwei Cai, Xuesong Li, Ji Won Suk, Jeffrey R. Potts, Rodney S. Ruoff, Graphene and graphene oxide: synthesis, properties, and applications, Adv. Mater. 22 (2010) 3906–3924, https://doi.org/10.1002/adma.201001068.
[43] Karthikeyan Krishnamoorthy, Murugan Veerapandian, Kyusik Yun, S.-J. Kim, The chemical and structural analysis of graphene oxides with different degrees of oxidation, Carbon 53 (2013) 38–49, https://doi.org/10.1016/j.carbon.2012.10.013.
[44] Jong Hun Kang, Taehoon Kim, Jaeyoo Choi, Jisoo Park, Yern Seung Kim, Mi Se Chang, Haesol Jung, Kyung Tae Park, Seung Jae Yang Chong Rae Park, Hidden second oxidation step or Hummers method, Chem. Mater. 28 (2016) 756–764, https://doi.org/10.1021/acs.chemmater.5b03700.
[45] Hsin-Cheng Hsu, Indrajit Shown, Hsieh-Yu Wei, Yu-Chung Chang, He-Yun Du, Yan-Gu Lin, Chi-Ang Tseng, Chen-Hao Wang, Li-Chyong Chen, Yu-Chuan Lin, Graphene oxide as a promising photocatalyst for CO_2 to metanol conversion, Nanoscale 5 (2013) 262–268, https://doi.org/10.1039/c2nr31718d.
[46] G. Barth, R. Linder, C. Bryson, Advances in charge neutralization for XPS measurements of nonconducting materials, Surf. Interface Anal. 11 (1988) 307–311, https://doi.org/10.1002/sia.740110607.
[47] G. Witek, M. Noeske, G. Mestl, Sh Shaikhutdinov, R.J. Behm, Interaction of platinum colloids with single crystalline oxide and graphite substrates: a combined AFM, STM and XPS study, Catal. Lett. 37 (1996) 35–39, https://doi.org/10.1007/BF00813516.
[48] David Briggs, Beamson Graham, Primary and secondary oxygen-induced X1s binding energy shifts in x-ray photoelectron spectroscopy of polymers, Anal. Chem. 64 (1992) 1729–1736, https://doi.org/10.1021/ac00039a018.
[49] M.K. Weldon, P. Uvdal, Decoupling of vibrational modes as a structural tool: coverage-induced reorientation of methoxide on Mo(1 1 0), J. Chem. Phys. 103 (1995) 5075–5084, https://doi.org/10.1063/1.470594.
[50] F. Solymosi, A. Berkó, Z. Tóth, Adsorption and dissociation of CH_3OH on clean and K-promoted Pd(1 0 0) surfaces, Surf. Sci. 285 (1993) 197–208, https://doi.org/10.1016/0039-6028(93)90430-R.
[51] X.D. Peng, M.A. Barteau, Spectroscopic characterization of surface species derived from HCOOH, CH_3COOH, CH_3OH, C_2H_5OH, $HCOOCH_3$, and C_2H_2 on MgO thin film surfaces, Surf. Sci. 224 (1989) 327–347, https://doi.org/10.1016/0039-6028(89)90918-7.
[52] Hans G. Jenniskens, Paul W.F. Dorlandt, Malcom F. Kadodwala, Aart W. Kleyn, The adsorption of metanol on Ag (1 1 1) studied with TDS and XPS, Surf. Sci. 357–358 (1996) 624–628, https://doi.org/10.1016/0039-6028(96)00234-8.
[53] Omid Akhavan, Graphene nanomesh by ZnO nanorod photocatalysts, ACS Nano 4 (2010) 4174–4180, https://doi.org/10.1021/nn1007429.
[54] Aurora Doren, Michel J. Genet, Paul G. Rouxhet, Analysis of poly(ethylene terephthalate) (PET) by XPS, Surf. Sci. Spectra 3 (1994) 337–341, https://doi.org/10.1116/1.1247762.
[55] P.D. Schulze, S.L. Shaffer, R.L. Hance, D.L. Utley, Adsorption of water on rhenium studied by XPS, J. Vac. Sci. Technol., A 97 (1) (1983) 97–99, https://doi.org/10.1116/1.572321.
[56] Qiu-Ping Luo, Xiao-Yun Yu, Bing-Xin Lei, Hong-Yan Chen, Dai-Bin Kuang, Cheng-Yong Su, Reduced graphene oxide-hierarchical ZnO hollow sphere composites with enhanced photocurrent and photocatalytic activity, J. Phys. Chem. C 116 (2012) 8111–8117, https://doi.org/10.1021/jp2113329.
[57] Alex W. Robertson, Alicja Bachmatiuk, Yimin A. Wu, Franziska Schäffel, Bernd Rellinghaus, Bernd Büchner, Mark H. Rümmeli, H. Jaime, Warner, Atomic structure of interconnected few-layer graphene domains, ACS Nano 5 (8) (2011) 6610–6618, https://doi.org/10.1021/nn202051g.
[58] Kenji Yamazaki, Yosuke Maehara, Kazutoshi Gohara, Characterization of TEM moiré patterns originating from two monolayer graphenes grown on the front and back sides of a copper substrate by CVD method, J. Phys. Soc. Jpn. 87 (2018) 061011, , https://doi.org/10.7566/JPSJ87.061011.
[59] Manoj K. Singh, Elby Titus, Gonçalves Gil, A. Paula, A.P. Marques, Igor Bdikin, Andrei L. Kholkin, J. José, A. Gracio, Atomic-scale observation of rotational misorientation in suspended few-layer graphene sheets, Nanoscale 2 (2010) 700–708, https://doi.org/10.1039/b9nr00256a.
[60] From: http://www.inven.nl/documenten/PCD03_handleiding.pdf, consulted the april 23th, 2017.
[61] N.M. Moscardo-Levelut, V. Plichon, Sulfur chemistry in equimolar NaOH-H_2O melt. II. Chemical reactions between sulfur, sulfide, polysulfides, and oxyanions, J. Electrochem. Soc. 131 (1984) 1545–1551, https://doi.org/10.1149/1.2115907.
[62] Herman V. Tartar, The reaction between sulfur and calcium hydroxide in aqueous solution, J. Am. Chem. Soc. 36 (3) (1914) 495–498, https://doi.org/10.1021/ja02180a005.
[63] Yanyuan Zhao, Kun Ting Eddie Chua, Chee Kwan Gan, Jun Zhang, Bo Peng, Zeping Peng, Qihua Xiong, Phonons in Bi_2S_3 nanostructures: Raman scattering and first-principles studies, Phys. Rev. B 84 (2011) 205330, https://doi.org/10.1103/PhysRevB.84.205330.
[64] P. Larson, V.A. Greanya, W.C. Tonjes, Rong Liu, S.D. Mahanti, Electronic structure of Bi_2X_3 (X = S, Se, T) compounds: comparison of theoretical calculations with photoemission studies, Phys. Rev. B 65 (2002) 085108, , https://doi.org/10.1103/PhysRevB.65.085108.
[65] Robert J. Levis, Zhicheng Jiang, Nicholas Winograd, Thermal decomposition of CH_3OH adsorbed on Pd{1 1 1}: a new reaction pathway involving CH_3 formation, J. Am. Chem. Soc. 111 (1989) 4605–4612, https://doi.org/10.1021/ja00195a013.
[66] S. Hoste, D.F. van de Vondel, G.P. van der Kelen, XPS Spectra of organometallic phenyl compounds of P, As, Sb and Bi, J. Electron. Spectrosc. Relat. Phenom. 17 (1979) 191–195, https://doi.org/10.1016/0368-2048(79)85040-9.
[67] Kiyotaka Uchida, Akimi Ayame, Dynamic XPS measurements on bismuth molybdate surfaces, Surf. Sci. 357–358 (1996) 170–175, https://doi.org/10.1016/0039-6028(96)00083-0.
[68] Mohamed M. Chehimi, Michel Delamar, X-Ray Photoelectron Spectroscopy of Merocyanine Dyes. Part VIII. Partial charge and conjugation of heteroatoms in the electroattractor rings, J. Electron. Spectrosc. Relat. Phenom. 50 (1990) c25–c32, https://doi.org/10.1016/0368-2048(90)87082-Y.
[69] Thomas P. Debbies, Wayne Rabalais, X-ray photoelectron spectra and electronic structure of Bi_2X_3 (X = O,S,Se,Te), Chem. Phys. 20 (1977) 277–283, https://doi.org/10.1016/0301-0104(77)85033-7.
[70] Wayne E. Morgan, Wojciech J. Stec, John R. van Wazer, Inner-orbital binding energy shifts of antimony and bismuth compounds, Inorg. Chem. 12 (1973) 953–955, https://doi.org/10.1021/ic50122a054.
[71] B.V.R. Chowdari, Rong Zhou, The influence of Bi_2O_3 on yLi_2O·(1-y) {xBi_2O_3(1-x) Bi_2O_3} glass system, Solid State Ionics 86–88 (1996) 527–533, https://doi.org/10.1016/0167-2738(96)00188-9.
[72] Xueping Xu, C.M. Friend, The role of coverage in determining adsorbate stability: phenol reactivity on Rh (1 1 1), J. Phys. Chem. 93 (1989) 8072–8080, https://doi.org/10.1021/j100361a021.
[73] Huiyan Fan, Guonian Wang, Lili Hu, Infrared, Raman and XPS spectroscopic studies of Bi_2O_3-B_2O_3-Ga_2O_3 glasses, Solid State Sci. 11 (2009) 2065–2070, https://doi.org/10.1016/j.solidstatesciences.2009.09.007.
[74] Husnu Koc, Kaci Ozisik, Engin Deligöz, Amirullah M. Mamedov, Ekmel Ozbay, Mechanical, electronic, and optical properties of Bi_2S_3 and Bi_2Se_3 compounds: first principle investigations, J. Mol. Model. 20 (2014) 2180, https://doi.org/10.1007/

s00894-014-2180-1.
[75] Marina R. Filip, Christopher E. Patrick, Feliciano Giustino, GW quasiparticle band structures of stibnite, antimonselite, bismuthinite, and guanajuatite, Phys. Rev. B 87 (2013) 205125, https://doi.org/10.1103/PhysRevB.87.205125.
[76] Si-Qi Zhan, Hui Wan, Liang Xu, Wei-Qing Huang, Gui-Fang Huang, Jin-Ping Long, P. Peng, Native vacancy defects in bismuth sulfide, Int. J. Mod. Phys. B 23 (2014) 1450150, https://doi.org/10.1142/S0217979214501501.
[77] Ehsan Zahedi, Hydrostatic pressure effects on the electronic, optical, and photocatalytic properties of ribbon-like Bi_2S_3: a DFT study, Superlattice. Microst. 81 (2015) 49–63, https://doi.org/10.1016/j.spmi.2014.12.036.